Korean J. Chem. Eng., 38(1), 22-31 (2021)
DOI: 10.1007/s11814-020-0678-z

pISSN: 0256-1115
eISSN: 1975-7220

Ampicillin adsorption onto amine-functionalized magnetic graphene oxide: synthesis, characterization and removal mechanism

Hoang Thu Ha*, Tran Dinh Minh*,†, Ha Minh Nguyet, and Ajit Kumar Sharma*****

*VNU University of Education, Vietnam National University, Hanoi, Vietnam
**Institute for Tropical Technology, 18 Hoang Quoc Viet, Hanoi, Vietnam
***School of Chemical Engineering and Physical Science, Lovely Professional University Phagwara, Punjab 144411, India
(*Received 3 May 2020 • Revised 11 September 2020 • Accepted 18 September 2020*)

Abstract−There are various chemical, physical and biological methods that have been applied to remove antibiotic residuals from aqueous environment. We investigated the removal of ampicillin (AMP) by a novel nanometer-size Fe_3O_4/graphene oxide/aminopropyltrimethoxysilane (FGOA). Based on the sol-gel method, the graphene oxide (GO) was first modified by aminopropyltrimethoxysilane (APTMS) to form GOA material containing both acidic and basic surface functional groups. The nanomagnetic iron oxide was then decorated to the GOA surface at various weight ratios by ultra-sonication in ethanol, resulting in different FGOA samples. The as-synthesized FGOA had single-layer structure and parallel array-like well-distributed Fe_3O_4. In laboratory-scale, the AMP treatment efficiency by FGOA with the ratio of Fe_3O_4 : GOA as 1 : 5 ratio reached the highest value around 94% within 100 min and only lost 1% after five regeneration cycles. The maximum adsorption capacity of FGOA was 294 mg g^{-1}, significantly much higher than the previously published materials applied to AMP uptake. Interestingly, the optimum pH of FGOA ranged extensively from 4 to 9, revealing high application potential to real wastewater without any pH adjustment. The reasonable mechanism might be mainly attributed to electrostatic attraction, hydrophilic, and π-π interaction.

Keywords: FGOA, Ampicillin Removal, Basic Modified Graphene Oxide, Magnetic Properties

INTRODUCTION

Antibiotics are medicines used to inhibit the growth of, or destroy, the bacteria in the prevention and treatment of infections. However, antibiotics have been overused in the treatment of diseases for both human and farm animals, leading to an emerging threat throughout the world: antibiotic resistance [1]. This term describes the ability of bacteria to grow, multiply and cause diseases within the host even when exposed to antibiotics. Antibiotic resistance results in higher medical costs, prolonged hospital stays, and increased mortality in Vietnam hospitals [2,3]. Particularly, more than 750,000 deaths every year are blamed on resistant germs and the number is predicted to rise dramatically if radical actions are not taken. Considering the formation pathways of resistance, the germs can be "trained" on how to fight the antibiotics by the excess drugs discharged from the human or animal body into the aquatic environment. Hence, one of the most effective resistance-control strategies is the treatment of antibiotic residuals in wastewater [4-6].

Ampicillin (AMP) was the first aminopenicillin with a broad spectrum against both Gram positive and Gram negative bacteria (Fig. 1) [7]. Due to its less toxicity and side effects compared to other antibiotics, AMP is generally used for pregnant women, lactating mothers and newborns [8]. Moreover, AMP covers antibiotics used in agriculture as infection treatment and growth promoter, ensuring farm productivity. Because of extensive use over recent decades,

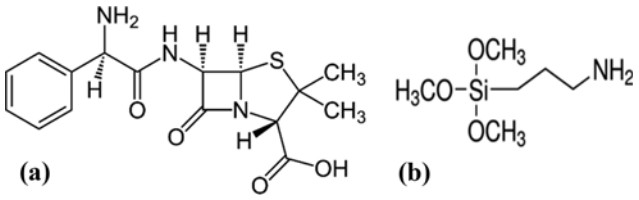

Fig. 1. (a) Chemical structure of AMP and (b) APTMS.

a fair quantity of AMP was detected in wastewater, resulting in AMP resistant genes and impacts on the activity of next-generation antibiotics in the penicillin family. Markedly, around 35-40% of E.Coli isolates and more than 95% of K.Pneumonia isolates are resistant to AMP [9]. Some studies have indicated that penicillin antibiotics are hardly biodegraded. Therefore, it is essential to remove the AMP accumulated in wastewater.

Among various methods of treatment of water pollution, adsorption has attracted the great interest of researchers for its low cost and simple operation. Different adsorbents were examined to remove the AMP residuals, including NH_2-SiO_2 [10], ZnO [11], TiO_2 [12], bentonite [13], activated carbon/H_2O_2, clay supported iron nanoparticles/Ni bimetallic nanoparticles [14], granular activated carbon [15], Bi_2O_3/BiOCl supported on graphene sand composite and chitosan [16]. However, these materials still show some drawbacks that cannot be scaled up for real application, such as complicated synthesis, poisonous by-products, difficult recovery and pH adjustment requirement [17-19].

Graphene oxide (GO) is a well-known adsorbent because of its efficiency, low production cost, high biocompatibility, large specific

†To whom correspondence should be addressed.
E-mail: minhtd.hes@vnu.edu.vn, dinhminh2609@gmail.com

surface area, various surface functional groups and modifiability [20]. Despite all advantages, GO does not satisfy application demand since it is difficult to recover from treated effluents. In general, centrifugation and filtration methods are used to separate the adsorbent material from aqueous solution [21]. These applications are time-consuming and require extra cost, as compared with traditional centrifugation and filtration methods, magnetic separation method is an efficient, fast and economic method for the separation of magnetic adsorbents from the medium after the adsorption treatment of pollutants is completed [22,23]. Other literatures also concluded that the novel graphene-based materials increased solar storage capacity by up to 3,000% [24]. The issue that scientists are always concerned with is that after being obtained, it must be stored so that energy is not lost or leaked over time [25-29]. This problem was solved when the researchers switched to graphene-based supercapacitors with ultra-fast charging technology and releasing energy into large arrays [30]. The magnetic iron oxide nanoparticles are usually supplemented to the substrate to facilitate the retake. For enhancing the removal efficiency of the specific contaminant, the binary material Fe_3O_4/GO needs to be further modified [31, 32]. Thus, this study developed a nanostructured composite of Fe_3O_4/graphene oxide/aminopropyltrimethoxysilane (FGOA) for the treatment of AMP with four principal objectives: (i) fabricate environment-friendly FGOA nanomaterial by simple routine based on sol-gel method, (ii) investigate the influence of FGOA at different conditions on the elimination of AMP in both laboratory and actual samples, (iii) provide a reasonable description of FGOA characteristics as well as a plausible mechanism of AMP adsorption over FGOA and finally, (iv) evaluate the reusability of FGOA [33]. The obtained results reveal the extensive application potential of the novel FGOA.

MATERIALS AND METHODS

1. Preparation of FGOA

All chemicals were ordered from Sigma-Aldrich (South Korea) and used as received. First, GO was prepared by an improved method of the research group of Professor Tour and colleagues at Rice University (USA) in a slight modification [34]. In brief, a mixture of concentrated sulfuric acid and phosphoric acid (9 : 1 volume ratio) was added to a mixture of graphite flakes and $KMnO_4$ (1 : 6 wt ratio). The reaction mixture was heated to 50 °C and stirred for 12 h. After that, the solution was cooled to room temperature (RT) and poured onto the ice prior to adding 3 mL of H_2O_2 30%. The filtrate was centrifuged at 4,000 rpm for 4 h and the supernatant was decanted out. The obtained solid was washed by deionized (DI) water, HCl 30% and ethanol, respectively. The material was then coagulated by ether, collected by filter membrane and dried overnight at 105 °C.

Second, the magnetic iron oxide was synthesized *via* the conventional co-precipitation method [35]. A solution containing Fe (II) and Fe (III) sulfate (1 : 1 mole ratio) was heated to 95 °C and instantly stirred at 700 rpm. A sufficient of aqua ammonium 28% was added to the system. The precipitation was collected by magnet, washed by DI water and ethanol for several times, then calcinated under nitrogen atmosphere at 400 °C for 6 h.

Third, the as-synthesized GO and APTMS were dispersed in ethanol by ultra-sonication at 90 °C for 4 h to form GO/APTMS (GOA) based on the sol-gel method. After washing to eliminate the excess of APTMS, the binary material GOA was redispersed in ethanol with Fe_3O_4 at different weight ratios (1 : 2, 1 : 3, 1 : 4, 1 : 5, 1 : 6, 1 : 7) by ultra-sonication to obtain the final FGOA products.

2. Sample Characterization

The surface morphology, pore diameter, and element composition of FGOA were determined by field emission scanning electron microscopy (FE-SEM imaging, EDX, JEOL/7000). Sample was covered with gold sputter coater and observed in an SEM operating at 10.0 kV. The elemental distribution (mapping) was conducted using energy dispersive X-ray system. The crystal structure of the sample was observed by transmission electron microscopy (TEM, JOEL, JEM-2010, Japan). Brunauer-Emmett-Teller (BET) specific surface area and pore volume were calculated using an ASAP/2020, Japan analyzer. The crystal phases of the material were determined by X-ray diffractometer (XRD-6100 Shimadzu, Japan). The saturated magnetization was detected by a superconducting quantum technique using a vibrating sample magnetometer (VSM-7307, SQUID) at RT. Zetasizer Nano ZS90, Malvern was used to identify the zeta potential of the material. For Fourier transform infrared spectroscopy (FTIR, IFS 66; Billerica, USA) analysis, 200 mg of KBr was prepared with 1.5 mg of sample, the spectra were recorded on a spectrometer in the mid IR range (4,000-400 cm^{-1}).

3. Adsorption Procedure

The AMP standard solutions at concentrations from 10 to 1,000 mg L^{-1} were prepared by dissolving an exact amount of AMP to DI water. In a typical experiment, 20 mg of FGOA was added to 20 mL of different AMP solutions at RT for 400 min. At a fixed time, a quantity of the suspension containing FGOA and AMP was taken out for measuring the remaining concentration. The absorbance of the standard solutions as well as that of the residuals after adsorption was measured by UV-Vis spectrometer (UV-2550, Shimadzu Japan) at 204 nm.

4. Reusable Ability of FGOA

To test the FGOA reusability for AMP adsorption, 5 mg of adsorbed-AMP/FGOA was washed into 50 mL flask containing of each solvent of H_2O, and C_2H_5OH, respectively. The suspension was thoroughly treated in magnetic stirrer in 24 h at 30 °C. Afterward, 10 mL of each sample containing in centrifuge tube rack was centrifuged for 5 min with a 4,000 rpm rotation rate, and the concentration of remain AMP in the supernatant was determined using UV-Vis spectrometer.

5. Data Processing

The adsorption capacity at equilibrium (q_e) and the removal efficiency (%R) were calculated by Eqs. (1) and (2), respectively:

$$q_e = \frac{(C_i - C_f) \times V}{m} \quad (1)$$

$$\%R = \frac{C_i - C_f}{C_i} \times 100 \quad (2)$$

where V is the volume of AMP solution (mL); m is the weight of FGOA (mg); C_i and C_f are the concentrations of AMP before

and after adsorption, respectively (mg L^{-1}). We examined two common kinetic models: pseudo-first-order and pseudo-second-order using Eqs. (3) and (4), respectively [19]:

$$\ln(q_e - q_t) = \ln q_e - k_1 t \quad (3)$$

$$\frac{t}{q_t} = \frac{1}{k_2 q_e^2} + \frac{t}{q_e} \quad (4)$$

Here, k_1 (min^{-1}) and k_2 (mg g^{-1} min^{-1}) represent the rate constants of pseudo-first-order and pseudo-second-order models, respectively; q_t is the adsorption capacity at a fixed time t (mg g^{-1}). We also investigated the adsorption behavior through two common models (Langmuir and Freundlich) by applying two corresponding Eqs. (5) and (6), respectively [17].

$$\frac{C_e}{q_e} = \frac{C_e}{q_{max}} + \frac{1}{b \cdot q_{max}} \quad (5)$$

$$\ln q_e = \ln K_F + \frac{1}{n} \ln C_e \quad (6)$$

where q_{max} is the maximum adsorption capacity (mg g^{-1}); b is Langmuir constant, relating to the free energy (L mg^{-1}); C_e is the AMP concentration at equilibrium (mg L^{-1}); K_F presents Freundlich constant associated with adsorption capacity [(mg g^{-1}) (mg $L^{-1})^{1/n}$], and n is the adsorption intensity.

RESULTS AND DISCUSSION

1. Material Characterization

1-1. Magnetization Properties of FGOA

Fig. 2(b) displays the XRD pattern of FGOA in the 2θ range of 0-100 °C. There are six specific peaks at positions 2θ=30°, 35°, 43°, 53°, 57° and 65° with the corresponding intensity of 220, 311, 400, 511, and 440, matching with the standard diffraction spectra (JCPDS Card No.019-0629) of the Fe_3O_4 crystal phase. This result proves the appearance of magnetic iron oxide nanoparticles in the FGOA [36].

Fig. 2(a) presents the magnetization curve from hysteresis loop of Fe_3O_4 and FGOA at magnetization field sweeping of ±15 kOe. Clearly, the magnetization curve appears as S-shape along with the saturation magnetization of Fe_3O_4 and FGOA as 18.1 and 9.2 emu g^{-1}, respectively, confirming the insertion of ferromagnetic iron oxide to FGOA. This also implies the high recoverability of FGOA

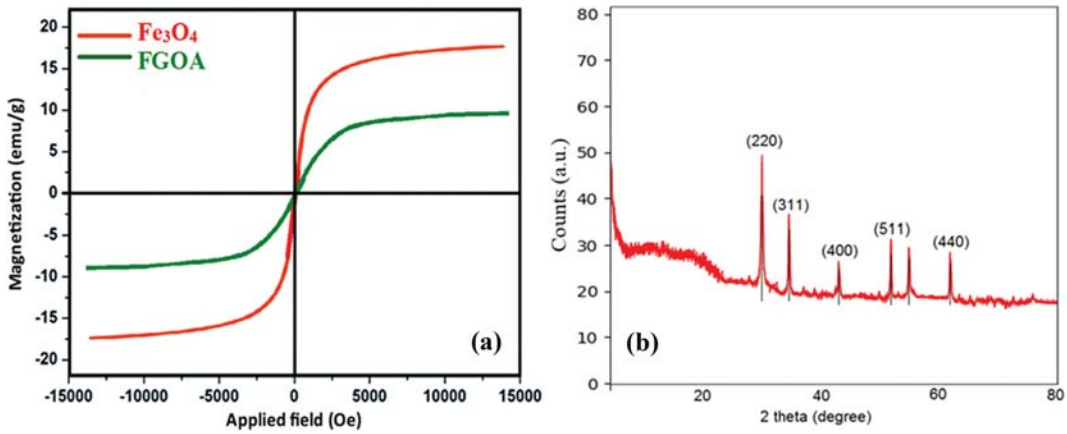

Fig. 2. (a) Saturation magnetization (M_s) value of Fe_3O_4 and FGOA, (b) XRD pattern of FGOA.

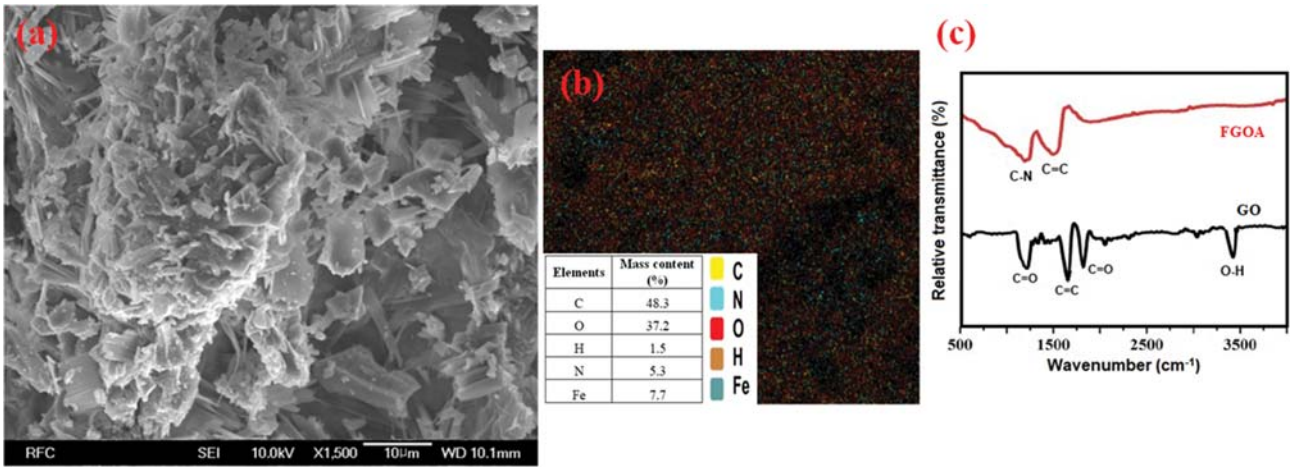

Fig. 3. (a) Compositional property obtained from SEM-EDS mapping analysis, (b) the textural properties of as-prepared FGOA, (c) FT-IR result.

after adsorption. The decrease in saturation magnetization value is due to the non-magnetic components in the material.

1-2. FE-SEM and Textural Studies

The as-prepared FGOA displays as an advanced material due to its uniform pore size, regular pore distribution and large specific surface area, which can be seen in Fig. 3(a).

The nanostructure with relatively smooth surface of FGOA nature was obtained by FE-SEM EDX imaging in Fig. 3(a) and 3(b). The FGOA surface displayed a uniform, homogeneous distribution, and equipped with the elemental analysis including of C, H, O, N and Fe. The existence of nitrogen and iron elements in the EDS mapping suggests the successful modification with Fe_3O_4 and APTMS.

1-3. FT-IR Spectroscopy

FT-IR is a critical analytical method for determining the surface functional groups in GO, and FGOA. Fig. 3(c) indicates the FT-IR spectrum of GO (black line) and FGOA (red line). Two notable absorption peaks at 1,726 and 1,189 cm^{-1} are clearly assigned to carbonyl (C=O) group stretching. The peak at 1,571 cm^{-1} is assumed for C=C bonds in GO and FGOA. The peak at 3,434 cm^{-1} is attributed to O-H stretching. A sharp stretching at 1,189 cm^{-1} in FGOA corresponds to C-N group, suggesting that the replacement of carbon atom by nitrogen atom. It is also evident that N-containing functional groups presented onto FGOA played an important role during AMP adsorption mechanism. As can be seen in Fig. 4(a), the amine group on APTMS was attached on the surface of GO to form the nitrogen group in the final product of FGOA. The C-N group in FGOA acted with AMP on the surface to form surface complexes adsorbed-AMP/FGOA, a bridging type of surface coordination (Fig. 4(b)) [37].

1-4. TEM and HR-TEM Imaging

As shown in the TEM image of the FGOA (Fig. 3(a)), the novel material has nanometer-size and spherical structure in a light black color. The HR-TEM image in the designed area reveals that the FGOA surface has a parallel grid crystal with a space of approximately 0.28 nm (Fig. 3(b)). In the view of active specific surface area, FGOA took advantage from both upper and lower external surfaces as well as all gullies and pleats on each surface. This interesting feature is attributed to the good dispersion of Fe_3O_4 nanoparticles on the GO surface.

1-5. Specific Surface Area and Porosity

Fig. 5(c) indicates the BET specific surface area and pore vol-

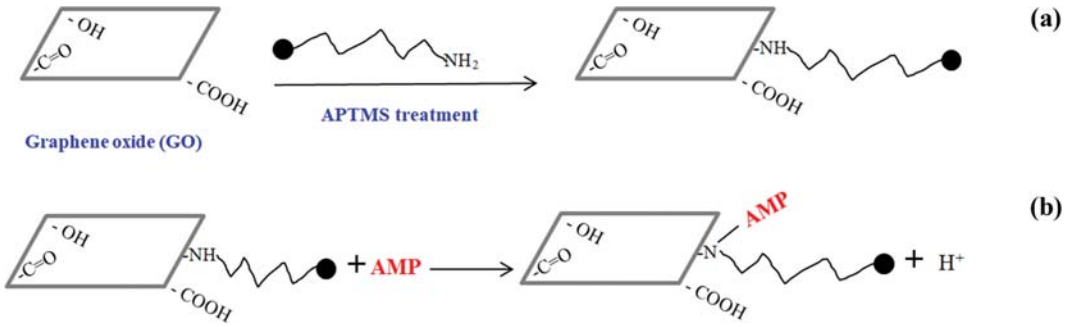

Fig. 4. (a) APTMS treatment with GO layer, (b) proposed interaction between AMP and FGOA surface.

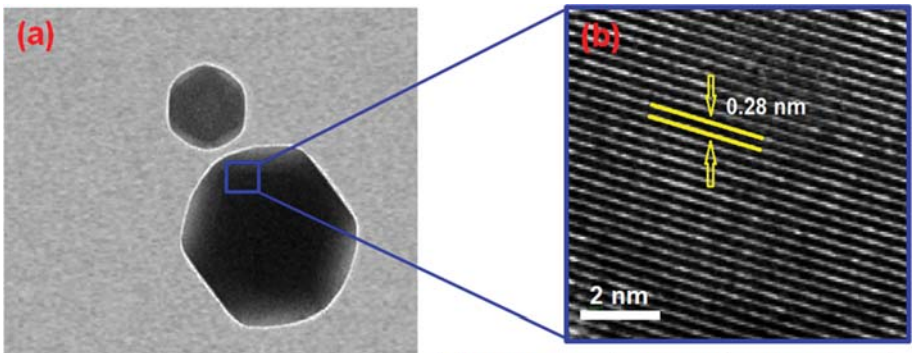

(c)

Weight ratios	BET specific surface area ($m^2 g^{-1}$)	Mesopore volume ($cm^3 g^{-1}$)
1 Fe_3O_4 : 1 GOA	318	0.23
1 Fe_3O_4 : 2 GOA	358	0.27
1 Fe_3O_4 : 3 GOA	390	0.31
1 Fe_3O_4 : 4 GOA	412	0.36
1 Fe_3O_4 : 5 GOA	445	0.41
1 Fe_3O_4 : 6 GOA	473	0.49
1 Fe_3O_4 : 7 GOA	501	0.58

Fig. 5. (a) TEM image, (b) HR-TEM, (c) the table of textual properties of FGOA.

ume of the FGOA samples with various weight ratios of Fe_3O_4 over GOA from 1 : 1 to 1 : 7. Obviously, FGOA has a porous structure, facilitating the adsorption process. The specific surface area and the pore volume of FGOA samples increased gradually with the increasing percentages of GOA. The BET of FGOA consisting of Fe_3O_4/GOA of 1 : 7 weight equivalent (wt equiv) enlarged about 160% (501 m^2 g^{-1}) in comparison with that consisting of 1 : 1 wt equiv (318 m^2 g^{-1}). Whilst, FGOA containing 87.5 wt% GOA had excessively double pore size (0.58 cm^3 g^{-1}) of that containing 50 wt% GOA (0.23 cm^3 g^{-1}). The changes in BET specific surface area and pore volume are reasonably due to the agglomeration of Fe_3O_4 on the GO. The pH value of the point of zero charge (pHpzc) of FGOA is 4.82, as shown in Fig. 6(b). By modifying GO surface, which contains acidic functional groups, by alkaline functional groups with basic properties, results in the pHpzc of FGOA achieved at 4.82. The relatively large BET specific surface area and specific crystal structure of FGOA might promote the enhanced AMP uptake.

1-6. Reasonable Insight into FGOA Linkages

As the FGOA synthesis was divided into two main steps, including the GO modification by APTMS and the GOA decoration by Fe_3O_4, the formation of linkages inside this novel material was so far different from the one-pot reaction. In the GOA synthesis stage, APTMS molecules could functionalize the GO surface by two separated pathways: (i) The silanization, in which the hydroxyl groups on GO surface attack and replace the methoxide groups on the silane, thus creating C-O-Si bonds (between GO and APTMS) and Si-O-Si bonds (between two adjacent APTMS) (as shown in Fig. 1). (ii) The proton exchange, in which the carboxylic groups on the GO surface play a role as a proton donor and the amine groups on the APTMS are proton acceptor, then forming electrostatic bonds -$COO^-H_3N^+$- (Fig. 6(a)).

During the second step, Fe_3O_4 were well-distributed under the influence of ultrasonic vibration. They could be attached to the GOA surface through multiple possible ways, mainly contributed by the hydroxyl groups surrounding magnetic nanoparticles. When dispersed into aqueous medium, the outermost iron atoms of Fe_3O_4 particles can serve as Lewis acid, coordinating with H_2O molecules. These coordinations are quickly hydrolyzed to form hydroxyl groups functionalizing the Fe_3O_4 surface. The active -OH groups allow magnetic particles to bond with GO both directly and indirectly. (iii) the hydrogen bonding among hydroxyl groups on GO and Fe_3O_4, (iv) the bridging through covalent bonds Fe-O-Si with APTMS. Particularly, APTMS molecules which functionalized the GO surface as the (ii) pathway remained free -$Si(OCH_3)_3$ groups to react with the hydroxyl groups of Fe_3O_4. Due to complex incorporation of Fe_3O_4, APTMS and GO, FGOA surface is assigned to contain at least four active functional groups: amino, carboxyl, hydroxyl and silane. These groups play an essential role in the chemi-

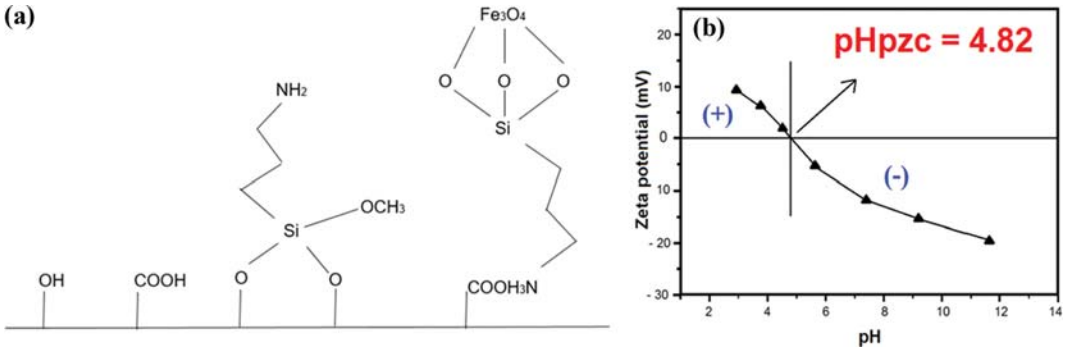

Fig. 6. (a) Surface functional groups, (b) pHpzc of FGOA.

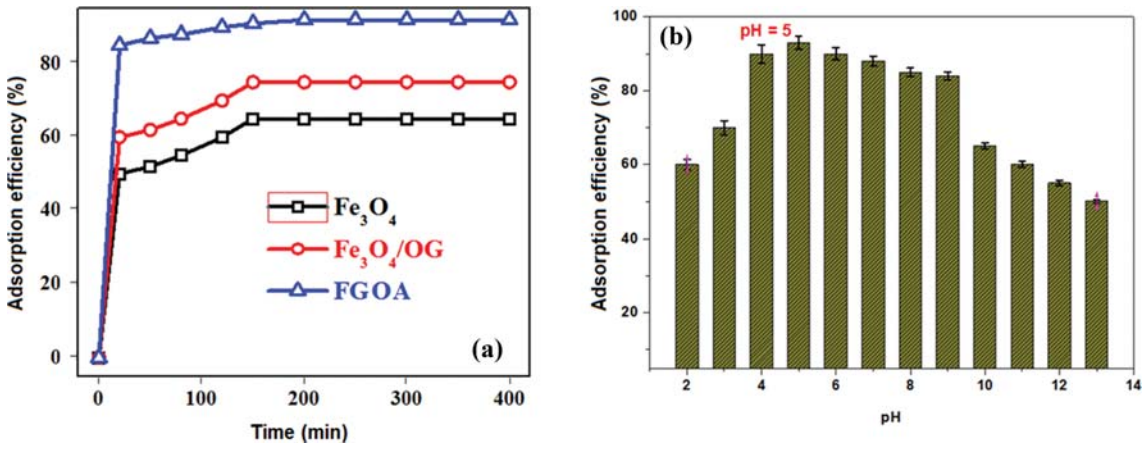

Fig. 7. (a) Adsorption efficiency comparison between FGOA and Fe_3O_4, Fe_3O_4/GO and (b) the effect of pH on AMP adsorption (concentration$_{AMP}$= 20 mg L^{-1}, m_{FGOA}=20 mg, t=30 min, T=25 °C).

cal characteristics of FGOA, that we will make clear later in this paper. We assume that, if three components of FGOA were mixed together, there would be two competitive functionalization processes since APTMS could simultaneously participate in the silanization on GO and Fe_3O_4 surface. By contrast, it is supposed that in FGOA, APTMS covered the GO surface and exclusively built a link with Fe_3O_4. Therefore, the obtained FGOA had a better-ordered structure, promoting the interaction surface of the adsorbent.

2. Removal of AMP Using FGOA

2-1. FGOA in Comparison with Its Precursors

To evaluate the material enhancement, we compared the AMP removal efficiency using Fe_3O_4, Fe_3O_4/OG and FGOA. As illustrated in Fig. 7(a), the elimination of AMP happened rapidly in the first 20 min and slowed gradually until the adsorption reached equilibrium state after 150 min for all materials. The maximum values that Fe_3O_4, Fe_3O_4/OG and FGOA achieved were approximately 63%, 72% and 94%, respectively. The result showed that the magnetic iron oxide and GO had adsorption ability to AMP; however, the efficiencies were not high enough. Obviously, the uptake efficiency using FGOA was significantly higher than that of Fe_3O_4 and Fe_3O_4/GO. It means that the combination in FGOA nanocomposite took benefits from the single materials.

2-2. Effect of pH on Removal Efficiency

We investigated the influence of pH on the AMP adsorption process by treating AMP solutions at a concentration of 20 mg L^{-1} using 20 mg of FGOA in different pH conditions (for 30 min and at 25 °C). The obtained data are interpreted in Fig. 7(b). As can be seen, the optimum pH range of AMP removal using FGOA was fairly wide, varying from 4 to 9 with the peak efficiency of 94% (at pH=5). Interestingly, this pH range is suitable for the actual wastewater condition, indicating that FGOA can be applied for polluted water treatment without pH adjustment. This result is consistent with the changes of the net surface charge of FGOA and the charge of AMP at different pH values, which we would like to discuss further in the proposed mechanism section.

2-3. Isothermal Modeling

Comparing the determination coefficients (R^2) of Langmuir model (0.99) and Freundlich model (0.97) as calculated and listed in the Table 1, we can conclude that the AMP uptake is better-fitted to the Langmuir model. Fig. 8(a) represents the Langmuir plot for AMP adsorption. Obviously, AMP molecules were distributed homogeneously on the FGOA surface as a monolayer, implying that the AMP uptake favorably follows chemisorption and a monolayer adsorption onto active sites of FGOA [37,38]. Similar isotherm results were reported for the adsorption isotherms of different pollutants by various adsorbents [39,40]. The value of n (1.76>1) calculated in the Freundlich model was evident that the AMP adsorption on FGOA is beneficial [41,42]. The adsorption isotherm parameters of both models were given below:

We listed the maximum adsorption capacity of some reported materials in the Table 2. As can be seen, the obtained maximum

Table 1. Langmuir and Freundlich isotherm parameters for adsorption of AMP

Langmuir			Freundlich		
q_{max} (mg g^{-1})	b (L mg^{-1})	R^2	K_F [(mg g^{-1}) (mg $L^{-1})^{1/n}$]	n	R^2
294	0.003	0.99	11.47	1.76	0.97

Table 2. q_{max} comparison with other work to remove AMP and β-lactam antibiotics

Adsorbent	q_{max} (mg g^{-1})	pH	Reference
H_2O_2/Activated carbon	80	3-5	[43]
Montmorillonite	141	5	[44]
NH_2/Activated carbon	206	3	[45]
Charcoal	178	3	
Granular activated carbon	204	6	[15]
NH_2/SiO_2	278	7.4	[10]
	333	7.4	
FGOA	**294**	**5**	**This work**

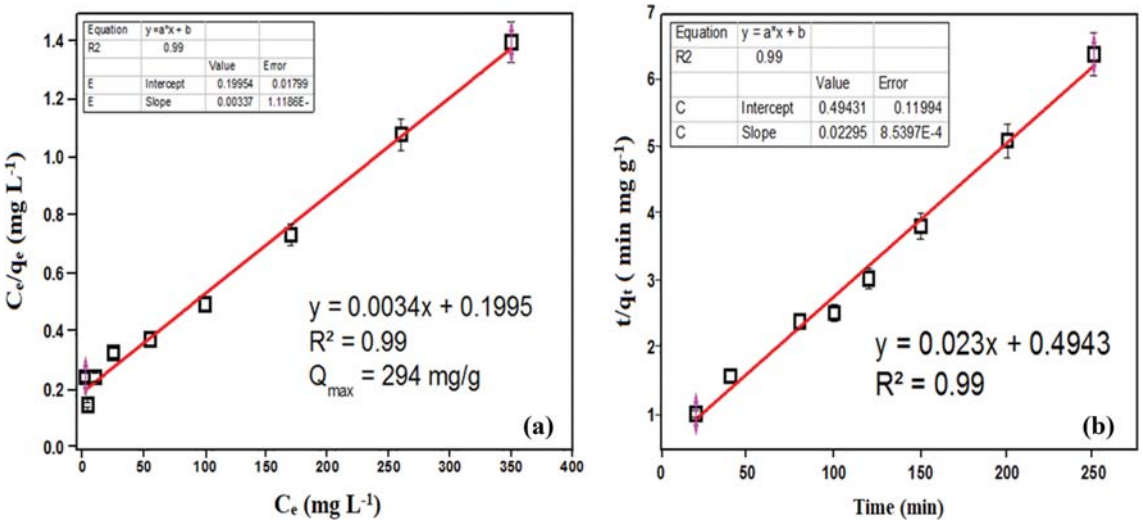

Fig. 8. The plot of (a) Langmuir adsorption isotherm, (b) pseudo-second-order model.

Table 3. Pseudo-second-order-model kinetic parameters

C_0 (mg L^{-1})	Pseudo-second-order model			
	$q_{e\text{-}exp}$ (mg g^{-1})	$q_{e\text{-}cal}$ (mg g^{-1})	k_2 (g mg^{-1} min^{-1})	R^2
30	12.27	12.33	5.68×10^{-1}	0.9972
50	21.43	21.56	5.11×10^{-1}	0.9903
100	40.19	40.23	4.96×10^{-1}	0.9977
150	65.84	65.94	4.24×10^{-1}	0.9895
200	89.20	89.43	3.79×10^{-1}	0.9999

$q_{e\text{-}exp}$: experimental adsorption capacity; $q_{e\text{-}cal}$: calculated adsorption capacity

adsorption capacity of FGOA was 294 mg g^{-1}, much higher than the previously published materials. Although the comparison is relative due to different experimental conditions, the result recommends a highly applicable potential of our novel composite.

2-4. Adsorption Kinetics for AMP

To verify the kinetics of AMP elimination by FGOA, we applied the pseudo-second-order model to the experimental data. Fig. 8(b) plots the t/q_t versus time (t); the determined coefficients of pseudo-second-order equation at different initial concentrations of AMP from 30 to 200 mg L^{-1} are reported in Table 3. The high relative coefficients alternating around 0.9895 and 0.9999 proved the suitability of pseudo-second-order for the AMP removal, revealing that chemi-sorption took place in the surface interaction. In literature, similar kinetic results were reported in the adsorption kinetic studies of some water pollutants onto adsorbent materials [46,47]. Moreover, it is obvious that the rate constants (k_2) decreased from 5.68×10^{-1} to 3.79×10^{-1} (g mg^{-1} min^{-1}) by the increasing initial AMP concentration. This fact contributes to the understanding of AMP sorption mechanism that the chemical interactions predominate, rather than physisorption.

2-5. Optimum Composition of FGOA

We applied FGOA samples with different ratios of Fe_3O_4 and GOA by weight for treatment of AMP solutions. The efficiency of AMP removal using seven FGOA samples over time is demonstrated in Fig. 9(a). Clearly, they all show highly effective removal from 50% (Fe_3O_4 : GOA=1 : 1) to 96% (Fe_3O_4 : GOA=1 : 5). The highest efficiency reached by the sample at medium position in the studied range suggests an interesting insight of each FGOA component's role. We would discuss this point in a further section.

Additionally, the adsorption equilibrium for entire FGOA samples reached within 100 min. This treatment time is suitable for large-scale application.

2-6. Thermodynamic Tests of Adsorption

Thermodynamic tests are a typical tool to determine whether the adsorption system of AMP by FGOA is spontaneous or not. The entropy (ΔS^o), Gibbs free energy (ΔG^o), and enthalpy (ΔH^o) change could be measured from the following Eqs. (7), (8) and (9) below:

$$\ln K_c = -\frac{\Delta H^o}{RT} + \frac{\Delta S^o}{R} \quad (7)$$

$$\Delta G^o = -RT\ln_K \quad (8)$$

$$\log K_c = \frac{\Delta S^o}{2.303R} - \frac{\Delta H^o}{2.303RT} \quad (9)$$

where K_c represents the equilibrium constant, T is Kelvin temperature (K), and R is gas constant (8.314 J K^{-1} mol^{-1}). ΔH^o and ΔS^o were measured from the slope and intercept of linear plots of $\log K_c$ as a function of 1/T. The plots were employed to determine the parameters of the thermodynamic constants in Table 4.

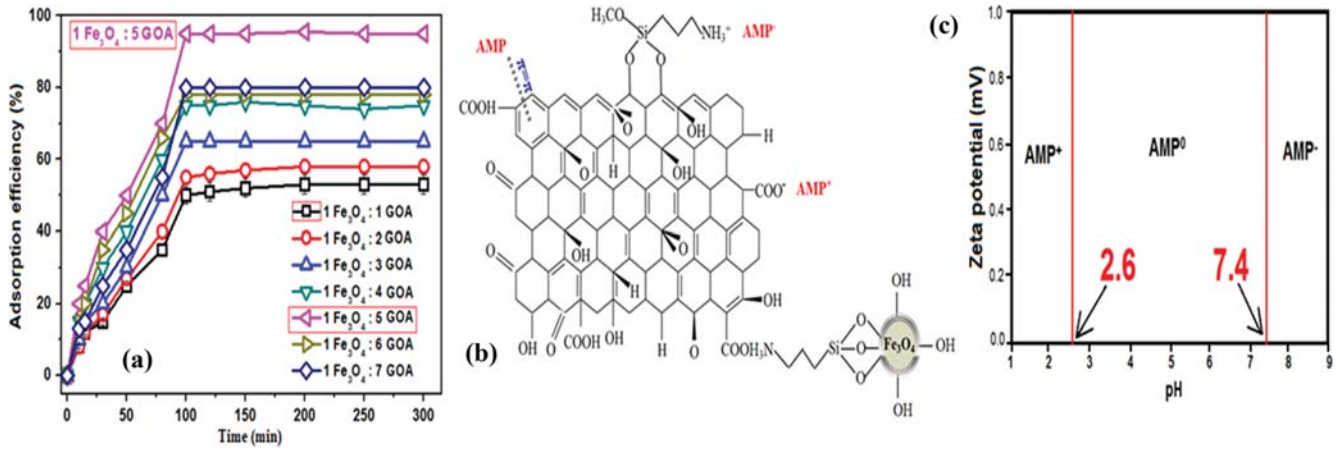

Fig. 9. (a) Effect of weight ratio of FGOA on the AMP removal (concentration$_{AMP}$=20 mg L^{-1}, m_{FGOA}=20 mg, pH=5, T=25 °C), (b) the chemical mechanism to remove AMP onto FGOA surface, (c) AMP existing species in different pH values.

Table 4. Thermodynamic parameters for the AMP adsorption using FGOA at an initial concentration ($C_{o\,AMP}$)=30 mg L^{-1}

$C_{o\,AMP}$ (mg L^{-1})	ΔH^o (kJ mol^{-1})	ΔS^o (J mol^{-1} K^{-1})	DG^o (kJ mol^{-1})		
			T=298 K	T=303 K	T=318 K
30	0.4	55.6	−2.3	−3.5	−5.8

ΔG^o was calculated among the sorption procedure at temperatures of 25, 35, and 45 °C, and to be more negative while the temperature increased. The negative values of ΔG^o were investigated for that the AMP adsorption of by FGOA is spontaneous and desired. The positive ΔS^o and ΔH^o revealed that the adsorption procedure is an endothermic activity, and the randomness at the solid-solution interface during the AMP adsorption [48].

3. Plausible Adsorption Mechanism

As mentioned when analyzing the thermal isotherms and kinetics information, the adsorption route favors chemical linking. Considering the structure of the adsorbent and adsorbate, the AMP elimination may be due to complex mechanisms, including electrostatic attraction, proton exchange, hydrogen bonding, π-π interaction. Fig. 9(b) illustrates possible adsorption pathways of AMP over FGOA.

3-1. Electrostatic Attraction

Fig. 9(c) presents the textural formula of AMP and its stable forms in different pH ranges; Fig. 6(b) displays isoelectric point (IEP or pHpzc) of FGOA. As can be seen, AMP molecule contains both basic and acidic functional groups. If pH of the surroundings is lower than 2.6 or higher than 7.4, AMP will be found in the protonated and deprotonated forms, respectively. Within the pH range from 2.6 to 7.4, AMP behaves as an electric dipole. While, the IEP of FGOA (4.8) shows that the adsorbent surface is negatively charged above pH=4.8 or, conversely, becomes positive below pH=4.8. Thus, the oppositely charged attraction occurs over an extensive pH range between the protonated AMP and negatively-charged FGOA (pH=2.6-4.8) or the deprotonated AMP and positively-charged FGOA (pH=4.8-7.4). In strongly acidic (pH<2.6) or strongly basic (pH>7.4) medium, AMP molecule and FGOA surface exist in the same charge, thus repulsing each other and leading to a decrease in the uptake efficiency.

3-2. Hydrogen Bonding

In both FGOA surface and AMP molecules, there are numerous functional groups containing active hydrogen atoms as well as highly electronegative elements, such as oxygen, nitrogen, silicon. This reason leads to various coupling ways of hydrogen bonds by which AMP is firmly attached to FGOA. Despite hydrogen bonds not being as durable as chemical or electrostatic attractions, they are considered as one among predominant mechanisms due to two following reasons. First, hydrogen bonds can occur at all pH conditions. Second, one hydrogen bond donor can engage some nearby hydrogen bond acceptors, and vice versa, one hydrogen bond acceptor can get involved with many neighboring hydrogen bond acceptors, supporting each other to generate stronger linkage.

3-3. π-π Interaction

Even in challenging conditions such as highly acidic (pH<2) and highly basic (pH>12), the adsorption efficiency was still over 50%, implying a connection between FGOA and AMP independent of electrostatic attraction. It is assumed that the inherent aromatic rings in FGOA surface and AMP are important building blocks to the adsorbent-adsorbate bonding. π-stacking is a well-known type of intermolecular interaction between two resonance systems, typically benzene rings which are found in FGOA surface and AMP molecules. In this case, the single-layer structure of FGOA undoubtedly enhanced the stacking interaction. Imaginatively, when π-π interaction pulls the AMP close to the FGOA surface, hydrogen and electrostatic bonds are formed more easily. Adversely, hydrogen and electrostatic bonds also assist the resonant ring of AMP in approaching the FGOA surface (Fig. 9(b)).

3-4. Roles of Fe_3O_4 Nanoparticles

Certainly, the BET specific area and pore volume as well as the quantity of functional surface groups increase with the increasing percentage of GOA in FGOA samples (as shown in Fig. 5(c)). This is attributed to the rise of the adsorption efficiency of FGOA samples with ratios of Fe_3O_4 : GOA from 1 : 1 to 1 : 5. However, FGOA containing higher proportion of GOA (Fe_3O_4 : GOA=1 : 6, and 1 : 7) resulted in less efficiency than expected. Taking into account the removal efficiency of FGOA and its precursors, we can see that Fe_3O_4 has fairly good adsorption ability to AMP due to the active surface hydroxyl groups. In basic and acidic solution, the hydroxyl on Fe_3O_4 surface appears in deprotonated ($-O^-$) and protonated ($-OH_2^+$) forms, respectively, generating electrostatic attraction to AMP. In neutral medium, the -OH group likely forms a hydrogen bond with AMP. Thus, decreasing the fraction of Fe_3O_4 in FGOA would limit its operation. Consequently, to utilize the adsorption ability of FGOA, we need to balance the effect of each component.

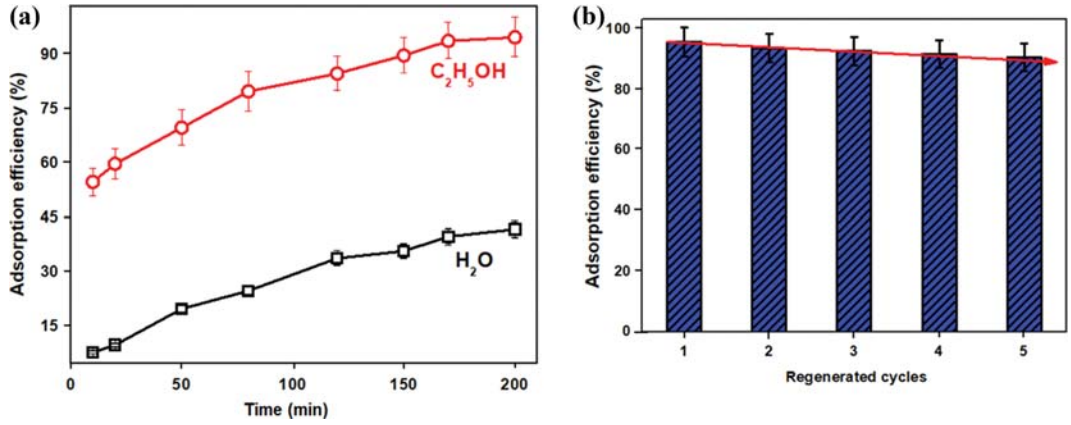

Fig. 10. (a) Desorption efficiency of AMP from FGOA by DI water and ethanol solvents, (b) reusable efficiency of FGOA by ethanol (m_{FGOA}= 20 mg, V_{AMP}=20 mL, concentration$_{AMP}$=20 mg L^{-1}, T=25 °C).

Table 5. Application in real wastewater

Composition	Unit	Before adsorption	After adsorption	Adsorption efficiency (%)
AMP	mg L^{-1}	50.0	19.5	61
Ni^{2+}	mg L^{-1}	9.1	4.6	49
Pb^{2+}	mg L^{-1}	11.3	7.4	34
pH	-	4.9	6.2	-
Color	-	Dark-brown	Light-brown	-

4. Reusability of FGOA

To assess the regeneration ability of FGOA, the research group of first co-author, Dr. Tran Dinh Minh (UEd, VNU), investigated the efficiency of the desorption process along with the efficiency of the re-used FGOA. Fig. 10(a) compares the desorption efficiency of two common eluting solvents (ethanol and water). Fig. 10(b) presents an analysis of the reusability of FGOA after five regenerated cycles. As can be seen, the desorption of FGOA using ethanol and water reached saturation at 93% and 40%, respectively, after 170 min. For these experimental data, ethanol was chosen to reactivate the FGOA for multiple times. The AMP-saturated composite was washed in ethanol for 24 h and applied to treat AMP for regeneration investigation. In each step, FGOA was quickly collected by a magnet. The fifth used efficiency of FGOA reduced 1%, insignificant compared to the first cycle.

5. Real Wastewater Study

To assess the practical applicability, FGOA was used to treat an actual sample extracted from livestock wastewater. The initial concentration of AMP in this sample was determined as 50 mg L^{-1}. The sample also contained various kinds of ions and compounds that are selectively listed in Table 5. The treatment efficiency of AMP, Ni^{2+} and Pb^{2+} was 61%, 49% and 34%, respectively. After treatment, the pH and the color of the actual sample markedly changed. Particularly, the pH increased from 4.9 to 6.2, implying that an amount of acidic species was removed. The primary brown color was faded to pale brown, indicating that some colored substances also were taken up. It suggested that FGOA has adsorption ability to other pollutants whether they are classified in the organics or inorganics. The decrease in removal efficiency of AMP (from 94% in laboratory conditions decreased to 61% in the actual environment) was due to the adsorption competition of different contaminants.

CONCLUSION

The novel nanocomposite Fe_3O_4/graphene oxide/aminopropyltrimethoxysilane was successfully synthesized at laboratory scale. The ampicillin maximum adsorption capacity was 294 mg g^{-1} with a wide active pH range from 4 to 9, close to the actual wastewater condition. The highest removal efficiency of AMP in standard solution and actual wastewater was 94% and 61%, respectively. The reused efficiency remained 93% after five regenerated cycles, presenting a high potential for practical application. The plausible and complex mechanism was attributed mainly to electrostatic attraction, hydrogen bonding, and π-π interaction. Each single adsorption pathway not only occurs overlapping, but also supports the others to increase the total removal efficiency.

ACKNOWLEDGEMENTS

This research is funded and granted by Vietnam National University (VNU), Hanoi, Vietnam.

COMPETING INTERESTS

The authors declare that we have no competing interests in this study.

DATA AVAILABILITY STATEMENT

All data, models, experiments and code used during the study appear in the submitted article.

REFERENCES

1. A. Anthony, F. Adekunle and S. Thor, *Phys. Chem. Earth*, **105**, 177 (2018)
2. L. Peters, L. Olson, D. T. Khu, S. Linnros, N. K. Le, H. Hanberger, N. T. Hoang, D. M. Tran and M. Larsson, *PloS One*, **14**, 5 (2019).
3. J. Seo, S. Y. Park, H.-H. Kim and C. Lee, *Frontiers in water-energy-nexus-nature-based solutions*, Advanced Technologies and Best Practices for Environmental Sustainability, Springer, 91 (2020).
4. S. Adhikari and D.-H. Kim, *Korean J. Chem. Eng.*, **36**, 468 (2019).
5. S.-H. Ji, W.-S. Jang, J.-W. Son and D.-H. Kim, *Korean J. Chem. Eng.*, **35**, 2474 (2018).
6. M. Zafar, J.-Y. Yun and D.-H. Kim, *Korean J. Chem. Eng.*, **35**, 567 (2018).
7. A. G. Ellis and G. R. Bloomberg, *Ann. Allergy Asthma Immunol.*, **122**, 422 (2019).
8. C. Dahl, H. Stigum, J. Valeur, N. Iszatt, V. Lenters, S. Peddada, J. V. Bjørnholt, T. Midtvedt, S. Mandal and M. Eggesbø, *Int. J. Epidemiol.*, **47**, 1658 (2018).
9. A. Fox-Lewis, J. Takata, T. Miliya, Y. Lubell, S. Soeng, P. Sar, K. Rith, G. McKellar, V. Wuthiekanun and E. McGonagle, *Emerg. Infect. Dis.*, **24**, 841 (2018).
10. V. Nairi, L. Medda, M. Monduzzi and A. Salis, *J. Colloid Interface Sci.*, **497**, 217 (2017).
11. E. S. Elmolla and M. Chaudhuri, *J. Hazard. Mater.*, **173**, 445 (2010).
12. E. S. Elmolla and M. Chaudhuri, *Desalination*, **252**(1-3), 46 (2010).
13. A. K. Rahardjo, M. J. J. Susanto, A. Kurniawan, N. Indraswati and S. Ismadji, *J. Hazard. Mater.*, **190**, 1001 (2011).
14. X. Weng, W. Cai, R. Lan, Q. Sun and Z. Chen, *Environ. Pollut.*, **236**, 562 (2018).
15. R. Y. H. Chia, *Removal of ampicillin and ciprofloxacin by GAC adsorption*, Nanyang Technological University Publication, Singapore (2018).
16. B. Priya, P. Raizada, N. Singh, P. Thakur and P. Singh, *J. Colloid Interface Sci.*, **479**, 271 (2016).
17. T. D. Minh and B.-K. Lee, *J. Mater. Cycles Waste Manag.*, **19**, 1022 (2017).
18. T. D. Minh and B.-K. Lee, *Environ. Sci. Pollut. Res.*, **25**, 21901 (2018).

19. T. D. Minh, B.-K. Lee and P. H. Linh, *Res. Chem. Intermed.*, **44**, 6515 (2018).
20. M. Aliofkhazraei, N. Ali, W. I. Milne, C. S. Ozkan, S. Mitura and J. L. Gervasoni, *Graphene science handbook: Electrical and optical properties*, Routledge & CRC Press Publications, United Kingdom (2016).
21. O. Duman, S. Tunç, B. K. Bozoğlan and T. G. Polat, *J. Alloys Compd.*, **687**, 370 (2016).
22. O. Duman, S. Tunç, T. G. Polat and B. K. Bozoğlan, *Carbohydr. Polym.*, **147**, 79 (2016).
23. O. Duman, C. Özcan, T. G. Polat and S. Tunç, *Environ. Pollut.*, **244**, 723 (2019).
24. K. S. Maan, A. Sharma, P. Nath, D.-V. N. Vo, H. T. Ha and T. D. Minh, *New dimensions in production and utilization of hydrogen*, Elsevier Publications, Netherlands, 321 (2020).
25. A. Pedico, A. Lamberti, A. Gigot, M. Fontana, F. Bella, P. Rivolo, M. Cocuzza and C. F. Pirri, *ACS Appl. Energy Mater.*, **1**, 4440 (2018).
26. W. C. Oh, K. Y. Cho, C. H. Jung and Y. Areerob, *Sci. Rep.*, **10**, 1 (2020).
27. L. Fagiolari and F. Bella, *Energy Environ. Sci.*, **12**, 3437 (2019).
28. J. Rakspun, Y.-J. Chiang, J.-Y. Chen, C.-Y. Yeh, V. Amornkitbamrung, N. Chanlek, V. Vailikhit and P. Hasin, *Sol. Energy*, **203**, 175 (2020).
29. L. L. Perreault, F. Colò, G. Meligrana, K. Kim, S. Fiorilli, F. Bella, J. R. Nair, C. Vitale-Brovarone, J. Florek and F. Kleitz, *Adv. Energy Mater.*, **8**, 1802438 (2018).
30. L. Zolin, J. R. Nair, D. Beneventi, F. Bella, M. Destro, P. Jagdale, I. Cannavaro, A. Tagliaferro, D. Chaussy and F. Geobaldo, *Carbon*, **107**, 811 (2016).
31. T. D. Minh, B.-K. Lee and M.-T. Nguyen-Le, *J. Environ. Manag.*, **209**, 452 (2018).
32. M.-T. Nguyen-Le, B.-K. Lee and D.-M. Tran, *J. Ind. Eng. Chem.*, **56**, 225 (2017).
33. N. T. Hanh, N. L. M. Tri, D. Van Thuan, M. H. T. Tung, T.-D. Pham, T. D. Minh, H. T. Trang, M. T. Binh and M. V. Nguyen, *J. Photochem. Photobiol. A: Chem.*, **382**, 111923 (2019).
34. D. C. Marcano, D. V. Kosynkin, J. M. Berlin, A. Sinitskii, Z. Sun, A. Slesarev, L. B. Alemany, W. Lu and J. M. Tour, *ACS Nano*, **4**, 4806 (2010).
35. H. Guan, J. Wang, S. Tan, Q. Han, Q. Liang and M. Ding, *Korean J. Chem. Eng.*, **37**, 1097 (2020).
36. M. Kalantari, M. Kazemeini and A. Arpanaei, *Mater. Res. Bull.*, **48**, 2023 (2013).
37. H. T. Ha, N. T. Huong, T. D. Minh, B.-K. Lee, E. R. Rene, T. V. Bao Linh, H. D. Minh, N. N. Quang, P. C. Mai and N. Q. Duc, *J. Environ. Chem. Eng.*, **146**, 04020060 (2020).
38. H. T. Ha, N. T. Huong, B. K. Lee, D. S. Duc, V. B. Trung, T. T. Kien, N. H. Anh, N. Q. Minh and T. D. Minh, *Res. Chem. Intermed.*, **46**, 5023 (2020).
39. O. Duman, S. Tunc and T. G. Polat, *Micropor. Mesopor. Mater.*, **210**, 176 (2015).
40. O. Duman, S. Tunç and T. G. Polat, *Appl. Clay Sci.*, **109**, 22 (2015).
41. S. Carabineiro, T. Thavorn-Amornsri, M. Pereira and J. Figueiredo, *Water Res.*, **45**, 4583 (2011).
42. S. Carabineiro, T. Thavorn-Amornsri, M. Pereira, P. Serp and J. Figueiredo, *Catal. Today*, **186**, 29 (2012).
43. G. Wang, T. Wu, Y. Li, D. Sun, Y. Wang, X. Huang, G. Zhang and R. Liu, *J. Chem. Technol. Biotechnol.*, **87**, 623 (2012).
44. D. Balarak, F. K. Mostafapour, H. Azarpira and A. Joghataei, *J. Pharm. Res. Int.*, **20**, 1 (2017).
45. Y. Wu, W. Liu, Y. Wang, X. Hu, Z. He, X. Chen and Y. Zhao, *Int. J. Environ. Res. Public Health*, **15**, 2652 (2018).
46. E. Ayranci and O. Duman, *Chem. Eng. J.*, **156**, 70 (2010).
47. O. Duman and E. Ayranci, *J. Hazard. Mater.*, **174**, 359 (2010).
48. M. Ghaedi, J. Tashkhourian, A. A. Pebdani, B. Sadeghian and F. N. Ana, *Korean J. Chem. Eng.*, **28**, 2255 (2011).